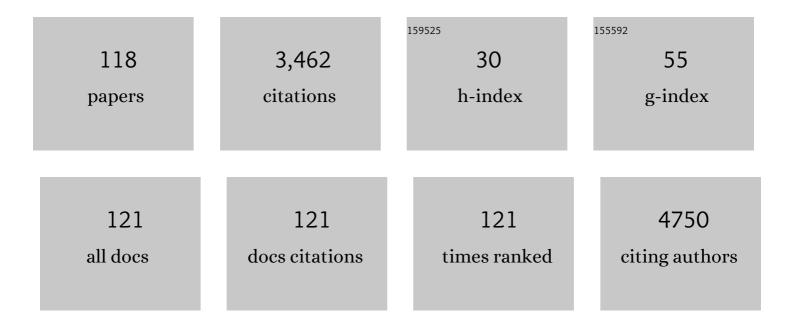
List of Publications by Year in descending order

Source: https://exaly.com/author-pdf/7870593/publications.pdf Version: 2024-02-01



SHICEDIL KIDVIL

#	Article	IF	CITATIONS
1	Deep Learning with Convolutional Neural Network for Differentiation of Liver Masses at Dynamic Contrast-enhanced CT: A Preliminary Study. Radiology, 2018, 286, 887-896.	3.6	446
2	Deep learning with convolutional neural network in radiology. Japanese Journal of Radiology, 2018, 36, 257-272.	1.0	243
3	Freeâ€breathing diffusionâ€weighted imaging for the assessment of inflammatory activity in Crohn's disease. Journal of Magnetic Resonance Imaging, 2009, 29, 880-886.	1.9	183
4	Spectrum of Epstein-Barr virus-related diseases: a pictorial review. Japanese Journal of Radiology, 2009, 27, 4-19.	1.0	148
5	Liver Fibrosis: Deep Convolutional Neural Network for Staging by Using Gadoxetic Acid–enhanced Hepatobiliary Phase MR Images. Radiology, 2018, 287, 146-155.	3.6	148
6	Noninvasive Bioluminescence Imaging of Luciferase Expressing Intracranial U87 Xenografts: Correlation with Magnetic Resonance Imaging Determined Tumor Volume and Longitudinal Use in Assessing Tumor Growth and Antiangiogenic Treatment Effect. Neurosurgery, 2006, 58, 365-372.	0.6	112
7	Diet and Abdominal Autofluorescence Detected by in Vivo Fluorescence Imaging of Living Mice. Molecular Imaging, 2008, 7, 7290.2008.0003.	0.7	95
8	Relationship Between Liver Function and Liver Signal Intensity in Hepatobiliary Phase of Gadolinium Ethoxybenzyl Diethylenetriamine Pentaacetic Acid-Enhanced Magnetic Resonance Imaging. Journal of Computer Assisted Tomography, 2010, 34, 362-366.	0.5	91
9	Detection of hepatocellular carcinoma by Gd-EOB-DTPA-enhanced liver MRI: Comparison with triple phase 64 detector row helical CT. European Journal of Radiology, 2011, 80, 310-315.	1.2	84
10	Deep learning for staging liver fibrosis on CT: a pilot study. European Radiology, 2018, 28, 4578-4585.	2.3	82
11	Breath-Hold T2-Weighted MRI of Hepatic Tumors: Value of Echo Planar Imaging with Diffusion-Sensitizing Gradient. Journal of Computer Assisted Tomography, 1998, 22, 364-371.	0.5	80
12	Predicting prognosis of resected hepatocellular carcinoma by radiomics analysis with random survival forest. Diagnostic and Interventional Imaging, 2018, 99, 643-651.	1.8	74
13	MR imaging of the biliary tract with Gd-EOB-DTPA: Effect of liver function on signal intensity. European Journal of Radiology, 2011, 77, 325-329.	1.2	72
14	Prediction of bone mineral density from computed tomography: application of deep learning with a convolutional neural network. European Radiology, 2020, 30, 3549-3557.	2.3	68
15	Comparison of subcutaneous and intraperitoneal injection of d-luciferin for in vivo bioluminescence imaging. European Journal of Nuclear Medicine and Molecular Imaging, 2009, 36, 771-779.	3.3	65
16	Quantitative analysis of the velocity and synchronicity of diaphragmatic motion: dynamic MRI in different postures. Magnetic Resonance Imaging, 2006, 24, 1325-1332.	1.0	61
17	Intravenous injection of umbilical cord-derived mesenchymal stromal cells attenuates reactive gliosis and hypomyelination in a neonatal intraventricular hemorrhage model. Neuroscience, 2017, 355, 175-187.	1.1	58
18	Fate of hypointense lesions on Gd-EOB-DTPA-enhanced magnetic resonance imaging. European Journal of Radiology, 2012, 81, 2973-2977.	1.2	56

SHIGERU KIRYU

#	Article	IF	CITATIONS
19	Deep learning to differentiate parkinsonian disorders separately using single midsagittal MR imaging: a proof of concept study. European Radiology, 2019, 29, 6891-6899.	2.3	51
20	Precision of quantitative computed tomography texture analysis using image filtering. Medicine (United States), 2017, 96, e6993.	0.4	49
21	Diet and abdominal autofluorescence detected by in vivo fluorescence imaging of living mice. Molecular Imaging, 2008, 7, 21-7.	0.7	49
22	Adaptive Iterative Dose Reduction in coronary CT angiography using 320-row CT: Assessment of radiation dose reduction and image quality. Journal of Cardiovascular Computed Tomography, 2012, 6, 318-324.	0.7	48
23	Magnetic resonance diffusion-weighted imaging in the characterization of pancreatic mucinous cystic lesions. Clinical Radiology, 2011, 66, 108-111.	0.5	41
24	Epstein–Barr virus-positive inflammatory pseudotumour and inflammatory pseudotumour-like follicular dendritic cell tumour. British Journal of Radiology, 2009, 82, e67-e71.	1.0	39
25	Impact of hepatocellular carcinoma heterogeneity on computed tomography as a prognostic indicator. Scientific Reports, 2017, 7, 12689.	1.6	39
26	Imaging prediction of nonalcoholic steatohepatitis using computed tomography texture analysis. European Radiology, 2018, 28, 3050-3058.	2.3	38
27	Quantitative computed tomography texture analysis for estimating histological subtypes of thymic epithelial tumors. European Journal of Radiology, 2017, 92, 84-92.	1.2	36
28	Source analysis of stimulus-preceding negativity constrained by functional magnetic resonance imaging. Biological Psychology, 2015, 111, 53-64.	1.1	35
29	Endometrial stromal sarcoma located in the myometrium with a lowâ€intensity rim on T2â€weighted images: Report of three cases and literature review. Journal of Magnetic Resonance Imaging, 2010, 31, 975-979.	1.9	33
30	Evaluation of Super Paramagnetic Iron Oxide-Enhanced Diffusion-Weighted PROPELLER T2-Fast Spin Echo Magnetic Resonance Imaging. Journal of Computer Assisted Tomography, 2006, 30, 197-200.	0.5	31
31	The Clinical Outcome of Small (<20 mm) Arterially Enhancing Nodules on MRI in the Cirrhotic Liver. American Journal of Gastroenterology, 2007, 102, 1654-1659.	0.2	28
32	Prediction of malignant glioma grades using contrast-enhanced T1-weighted and T2-weighted magnetic resonance images based on a radiomic analysis. Scientific Reports, 2019, 9, 19411.	1.6	27
33	Meandering Main Pancreatic Duct as a Relevant Factor to the Onset of Idiopathic Recurrent Acute Pancreatitis. PLoS ONE, 2012, 7, e37652.	1.1	26
34	Gaussia Luciferase for Bioluminescence Tumor Monitoring in Comparison with Firefly Luciferase. Molecular Imaging, 2011, 10, 7290.2010.00057.	0.7	24
35	Detection of liver metastasis: is diffusion-weighted imaging needed in Gd-EOB-DTPA-enhanced MR imaging for evaluation of colorectal liver metastases?. Japanese Journal of Radiology, 2012, 30, 648-658.	1.0	23
36	Precision of the measurement of CT numbers: comparison of dual-energy CT spectral imaging with fast kVp switching and conventional CT with phantoms. Japanese Journal of Radiology, 2012, 30, 34-39.	1.0	23

SHIGERU KIRYU

#	Article	IF	CITATIONS
37	Coronary CT angiography using the second-generation 320-detector row CT: assessment of image quality and radiation dose in various heart rates compared with the first-generation scanner. International Journal of Cardiovascular Imaging, 2013, 29, 1613-1618.	0.7	23
38	Evaluation of gadoxetate disodium as a contrast agent for mouse liver imaging: comparison with gadobenate dimeglumine. Magnetic Resonance Imaging, 2009, 27, 101-107.	1.0	22
39	Pancreas Duct Abnormalities in Patients with Ulcerative Colitis Inflammatory Bowel Diseases, 2005, 11, 903-908.	0.9	21
40	Timing of Imaging after D-Luciferin Injection Affects the Longitudinal Assessment of Tumor Growth Using In Vivo Bioluminescence Imaging. International Journal of Biomedical Imaging, 2010, 2010, 1-6.	3.0	20
41	Influence of hemodynamic parameters on coronary artery attenuation with 320-detector coronary CT angiography. European Journal of Radiology, 2012, 81, 230-233.	1.2	20
42	Reducing CT radiation exposure with organ effective modulation: A retrospective clinical study. European Journal of Radiology, 2016, 85, 1569-1573.	1.2	19
43	Retroportal main pancreatic duct with circumportal pancreas: radiographic visualization. Clinical Imaging, 2011, 35, 442-446.	0.8	17
44	Quantitative analysis of skeletal muscle mass in patients with rheumatic diseases under glucocorticoid therapy – Comparison among bioelectrical impedance analysis, computed tomography, and magnetic resonance imaging. Modern Rheumatology, 2015, 25, 257-263.	0.9	17
45	Impact of deep learning reconstruction on intracranial 1.5ÂT magnetic resonance angiography. Japanese Journal of Radiology, 2022, 40, 476-483.	1.0	17
46	Magnetic resonance imaging and diffusion tensor analysis of lymphomatoid granulomatosis of the brain. Acta Radiologica, 2006, 47, 509-513.	0.5	16
47	Quantitative computed tomography texture analyses for anterior mediastinal masses: Differentiation between solid masses and cysts. European Journal of Radiology, 2018, 100, 85-91.	1.2	16
48	Assessment of MRI Contrast Agent Kinetics via Retro-Orbital Injection in Mice: Comparison with Tail Vein Injection. PLoS ONE, 2015, 10, e0129326.	1.1	16
49	Prepancreatic postduodenal portal vein: a new hypothesis for the development of the portal venous system. Japanese Journal of Radiology, 2010, 28, 157-161.	1.0	15
50	Anticipation process of the human brain measured by stimulus-preceding negativity (SPN). The Journal of Physical Fitness and Sports Medicine, 2017, 6, 7-14.	0.2	15
51	PEGâ€poly(Lâ€lysine)â€based polymeric micelle MRI contrast agent: Feasibility study of a Gdâ€micelle contrast agent for MR lymphography. Journal of Magnetic Resonance Imaging, 2018, 47, 238-245.	1.9	15
52	Adaptive statistical iterative reconstruction for volume-rendered computed tomography portovenography: improvement of image quality. Japanese Journal of Radiology, 2010, 28, 700-706.	1.0	14
53	Diet and gastrointestinal signal on T1-weighted magnetic resonance imaging of mice. Magnetic Resonance Imaging, 2010, 28, 273-280.	1.0	14
54	Facial, verbal, and symbolic stimuli differently affect the right hemisphere preponderance of stimulusâ€preceding negativity. Psychophysiology, 2014, 51, 843-852.	1.2	13

#	Article	IF	CITATIONS
55	MRI assessment of lung parenchymal motion in normal mice and transgenic mice with sickle cell disease. Journal of Magnetic Resonance Imaging, 2008, 27, 49-56.	1.9	12
56	Efficacy of Double-Arterial Phase Gadolinium Ethoxybenzyl Diethylenetriamine Pentaacetic Acid-Enhanced Liver Magnetic Resonance Imaging Compared With Double-Arterial Phase Multi-Detector Row Helical Computed Tomography. Journal of Computer Assisted Tomography, 2009, 33, 887-892.	0.5	12
57	Increased prevalence of coronary artery calcification in patients with suspected pulmonary embolism1. Academic Radiology, 2003, 10, 840-845.	1.3	11
58	MR microscopy of the lung in small rodents. European Journal of Radiology, 2007, 64, 367-374.	1.2	11
59	Fluorescence Lymph Node Mapping in Living Mice Using Quantum Dots and a Compression Technique. Journal of Fluorescence, 2010, 20, 599-606.	1.3	11
60	Relationship between beat to beat coronary artery motion and image quality in prospectively ECG-gated two heart beat 320-detector row coronary CT angiography. International Journal of Cardiovascular Imaging, 2012, 28, 139-146.	0.7	11
61	Computed tomography and magnetic resonance imaging of a plexiform angiomyxoid myofibroblastic tumor: a case report. BMC Medical Imaging, 2017, 17, 7.	1.4	11
62	Breath-hold 3D magnetic resonance cholangiopancreatography at 1.5ÂT using a deep learning-based noise-reduction approach: Comparison with the conventional respiratory-triggered technique. European Journal of Radiology, 2021, 144, 109994.	1.2	11
63	Differentiation Between Hemangiomas and Cysts of the Liver with Single-Shot Fast-Spin Echo Image Using Short and Long TE. Journal of Computer Assisted Tomography, 2002, 26, 687-690.	0.5	10
64	Bioluminescent evaluation of the therapeutic effects of total body irradiation in a murine hematological malignancy model. Experimental Hematology, 2008, 36, 1634-1641.	0.2	10
65	Santorinicele without pancreas divisum pathophysiology: initial clinical and radiographic investigations. BMC Gastroenterology, 2013, 13, 62.	0.8	10
66	MDS cells impair osteolineage differentiation of MSCs via extracellular vesicles to suppress normal hematopoiesis. Cell Reports, 2022, 39, 110805.	2.9	10
67	Differentiation of adrenal tumors in patients with hepatocellular carcinoma: Adrenal adenoma versus metastasis. European Journal of Radiology, 2013, 82, 1213-1218.	1.2	9
68	Effects of Gadolinium Deposition in the Brain on Motor or Behavioral Function: A Mouse Model. Radiology, 2021, 301, 409-416.	3.6	9
69	Deep learning reconstruction for 1.5 T cervical spine MRI: effect on interobserver agreement in the evaluation of degenerative changes. European Radiology, 2022, 32, 6118-6125.	2.3	9
70	Clinical feasibility of an abdominal thin-slice breath-hold single-shot fast spin echo sequence processed using a deep learning-based noise-reduction approach. Magnetic Resonance Imaging, 2022, 90, 76-83.	1.0	9
71	Effect of temporal resolution on the estimation of left ventricular function by cardiac MR imaging. Magnetic Resonance Imaging, 2005, 23, 641-645.	1.0	8
72	Silent White Matter Lesion in Linear Scleroderma En Coup de Sabre. Journal of Computer Assisted Tomography, 2008, 32, 822-824.	0.5	8

#	Article	IF	CITATIONS
73	Interstitial MR Lymphography in Mice: Comparative Study with Gadofluorine 8, Gadofluorine M, and Gadofluorine P. Magnetic Resonance in Medical Sciences, 2012, 11, 99-107.	1.1	8
74	Shorter delay time reduces interpatient variability in coronary enhancement in coronary CT angiography using the bolus tracking method with 320-row CT. International Journal of Cardiovascular Imaging, 2013, 29, 185-190.	0.7	8
75	The effects of bolus supplementation of branched-chain amino acids on skeletal muscle mass, strength, and function in patients with rheumatic disorders during glucocorticoid treatment. Modern Rheumatology, 2017, 27, 508-517.	0.9	8
76	Application of CT texture analysis to assess the localization of primary aldosteronism. Scientific Reports, 2020, 10, 472.	1.6	8
77	Erdheim–Chester disease with an 18F-fluorodeoxyglucose-avid breast mass and BRAF V600E mutation. Japanese Journal of Radiology, 2014, 32, 282-287.	1.0	7
78	Gadoxetate disodium-induced tachypnoea and the effect of dilution method: a proof-of-concept study in mice. European Radiology, 2018, 28, 692-697.	2.3	7
79	Factors associated with the size of the adhesio interthalamica based on 3.0-T magnetic resonance images. Acta Radiologica, 2019, 60, 113-119.	0.5	7
80	Detection of Lung Tumors in Mice Using a 1-Tesla Compact Magnetic Resonance Imaging System. PLoS ONE, 2014, 9, e94945.	1.1	7
81	Feasibility of accelerated whole-body diffusion-weighted imaging using a deep learning-based noise-reduction technique in patients with prostate cancer. Magnetic Resonance Imaging, 2022, 92, 169-179.	1.0	7
82	Interstitial MR lymphography in mice with gadopentetate dimeglumine and gadoxetate disodium. Journal of Magnetic Resonance Imaging, 2011, 33, 490-497.	1.9	6
83	Effect of isoflurane anesthesia and hypothermia on the hepatic kinetics of Gdâ€EOBâ€DTPA: Evaluation using MRI of conscious mice. Journal of Magnetic Resonance Imaging, 2011, 34, 354-360.	1.9	6
84	The feasibility of halfcycle reconstruction in high heart rates in coronary CT angiography using 320-row CT. International Journal of Cardiovascular Imaging, 2013, 29, 907-911.	0.7	6
85	Coronary artery calcium score may be a novel predictor of COVID-19 prognosis: a retrospective study. BMJ Open Respiratory Research, 2021, 8, e000923.	1.2	6
86	Integrated Lymphography using Fluorescence Imaging and Magnetic Resonance Imaging in Intact Mice. Molecular Imaging, 2011, 10, 7290.2010.00049.	0.7	5
87	MR Imaging of Carcinosarcoma of the Liver using Gd-EOB-DTPA. Magnetic Resonance in Medical Sciences, 2014, 13, 117-121.	1.1	5
88	Motor and Nonmotor Components of Event-Brain Potential in Preparation of Motor Response. Journal of Behavioral and Brain Science, 2011, 01, 234-241.	0.2	5
89	Integrated Imaging Approach to Tumor Model Mice Using Bioluminescence Imaging and Magnetic Resonance Imaging. Molecular Imaging, 2010, 9, 7290.2010.00013.	0.7	4
90	Lymph Drainage from the Mammary Glands in Mice. Academic Radiology, 2011, 18, 512-517.	1.3	4

#	Article	IF	CITATIONS
91	Effect of saline flush on enhancement of proximal and distal segments using 320-row coronary CT angiography. European Journal of Radiology, 2013, 82, 1255-1259.	1.2	4
92	Hepatic Involvement of Histiocytic Sarcoma: CT and MRI Findings. Korean Journal of Radiology, 2016, 17, 758.	1.5	4
93	Clinical and CT features of ovarian torsion in infants, children and adolescents. International Journal of Gynecology and Obstetrics, 2022, 156, 444-449.	1.0	4
94	Voice, rhythm, and beep stimuli differently affect the right hemisphere preponderance and components of stimulus-preceding negativity. Biological Psychology, 2021, 160, 108048.	1.1	4
95	Radiomics with 3-dimensional magnetic resonance fingerprinting: influence of dictionary design on repeatability and reproducibility of radiomic features. European Radiology, 2022, 32, 4791-4800.	2.3	4
96	Commercially Available Deep-learning-reconstruction of MR Imaging of the Knee at 1.5T Has Higher Image Quality Than Conventionally-reconstructed Imaging at 3T: A Normal Volunteer Study. Magnetic Resonance in Medical Sciences, 2023, 22, 353-360.	1.1	4
97	Administration of Iodized Oil Resulted in Impaired Liver Function Due to Enhanced Portosystemic Shunting. CardioVascular and Interventional Radiology, 2004, 27, 282-4.	0.9	3
98	The natural history of streptozotocin-stimulated non-alcoholic steatohepatitis mice followed by Gd-EOB-DTPA-enhanced MRI: Comparison with simple steatosis mice. Magnetic Resonance Imaging, 2017, 38, 123-128.	1.0	3
99	Anomalous branching pattern of the portal vein: right posterior portal vein originating from the left portal vein. Surgical and Radiologic Anatomy, 2017, 39, 573-576.	0.6	3
100	Resectable primary pleural myxoid liposarcoma with a pedicle: report of a rare case and literature review. Journal of Thoracic Disease, 2017, 9, E183-E187.	0.6	3
101	Distortion correction in whole-body imaging of live mice using a 1-Tesla compact magnetic resonance imaging system. Japanese Journal of Radiology, 2011, 29, 353-360.	1.0	2
102	Prediction of the attenuation of the ascending aorta using bolus-tracking parameters and heart rate in coronary computed tomography angiography. European Journal of Radiology, 2012, 81, 3250-3253.	1.2	2
103	A pulmonary metastatic model of murine melanoma assessed by magnetic resonance imaging. Experimental Dermatology, 2017, 26, 619-621.	1.4	2
104	Integrated imaging approach to tumor model mice using bioluminescence imaging and magnetic resonance imaging. Molecular Imaging, 2010, 9, 163-72.	0.7	2
105	Long-term assessment of contrast effects of gadofluorine M and gadofluorine P in magnetic resonance imaging of mice. Japanese Journal of Radiology, 2012, 30, 86-91.	1.0	1
106	Influence of Indocyanine Green on Hepatic Gd-EOB-DTPA Uptake. Investigative Radiology, 2017, 52, 441-445.	3.5	1
107	Deep learning application in the oesophageal endoscopy. Journal of Medical Artificial Intelligence, 2019, 2, 22-22.	1.1	1
108	Whole-lesion histogram analysis of apparent diffusion coefficient for the assessment of non-mass enhancement lesions on breast MRI. Journal of Clinical Imaging Science, 2022, 12, 12.	0.4	1

#	Article	IF	CITATIONS
109	Radiation Protection of the Eye Lens in Fluoroscopy-guided Interventional Procedures. Interventional Radiology, 2022, 7, 44-48.	0.2	1
110	Quantitative Effect of Reducing Body Thickness on Visualizing Murine Deep Abdominal Lymph Nodes by In Vivo Fluorescence Reflectance Imaging. Journal of Fluorescence, 2011, 21, 1325-1329.	1.3	0
111	Physiological sources of stimulus-preceding negativity: Source analysis using fMRI and ERP. International Journal of Psychophysiology, 2014, 94, 200.	0.5	0
112	Early and late components of stimulus-preceding negativity prior to face, word, and symbol stimuli. International Journal of Psychophysiology, 2014, 94, 203-204.	0.5	0
113	The inhibitory effect of gadoxetate disodium on hepatic transporters: a study using indocyanine green. European Radiology, 2018, 28, 4128-4133.	2.3	0
114	Effects of negativity bias on amygdala and anterior cingulate cortex activity in short and long emotional stimulation paradigms. NeuroReport, 2021, 32, 531-539.	0.6	0
115	In vitro demonstration of melanoma metastasis in lymph nodes of prepared specimens using a light-emitting diode-based multispectral photoacoustic ultrasound imaging system. Journal of Medical Ultrasound, 2021, 29, 50.	0.2	0
116	Detection of Small Hepatic Lesions: Superparamagnetic Oxide-Enhanced Diffusion-Weighted T2 FSE Imaging. , 2009, , 213-219.		0
117	CT and clinical analysis of ovarian mucinous tumors in adolescent patients. Journal of Pediatric and Adolescent Gynecology, 2021, , .	0.3	0
118	Impaired Osteoblastic Differentiation of MSCs Suppresses Normal Hematopoiesis in MDS. Blood, 2020, 136, 17-18.	0.6	0